

1 Concurrent photochemical whitening and darkening of ambient 2 brown carbon

3 Qian Li¹, Dantong Liu^{1*}, Xiaotong Jiang¹, Ping Tian², Yangzhou Wu¹, Siyuan Li¹, Kang Hu¹, Quan Liu³,
4 Mengyu Huang², Ruijie Li², Kai Bi², Shaofei Kong⁴, Deping Ding²

5 ¹Department of Atmospheric Science, School of Earth Science, Zhejiang University, Hangzhou, 310027, China

6 ²Beijing Key Laboratory of Cloud, Precipitation and Atmospheric Water Resources, Beijing Meteorological Service, Beijing,
7 100089, China.

8 ³State Key Laboratory of Severe Weather & Key Laboratory of Atmospheric Chemistry of CMA, Chinese Academy of
9 Meteorological Sciences, Beijing, 100081, China

10 ⁴Department of Atmospheric Science, School of Environmental Science, China University of Geosciences, Wuhan, 430074,
11 China

12 *Correspondence to:* Dantong Liu (dantongliu@zju.edu.cn)

13 **Abstract.** The light-absorbing organic aerosol (OA), known as brown carbon (BrC), has important radiative impacts, however
14 its sources and evolution after emission remain to be elucidated. In this study, the light absorption at multiple wavelengths,
15 mass spectra of OA and microphysical properties of black carbon (BC) were characterized at a typical sub-urban environment
16 in Beijing. The absorption of BC is constrained by its size distribution and mixing state, being subtracted from total absorption
17 to obtain the absorption of BrC, then by applying the least-correlation of BC absorption with secondary BrC, the absorption
18 contributed by BC, primary BrC and secondary BrC was apportioned. The multi-linear regression analysis on the factorized
19 OA mass spectra indicated the OA from traffic and biomass burning emission contributed to primary BrC. Importantly, the
20 moderately oxygenated OA (O/C=0.62) was revealed to highly correlate with secondary BrC. These OA had higher nitrogen
21 content, in line with the nitrogen-containing functional groups detected by the Fourier transform infrared spectrometer. The
22 photooxidation was found to result in reduced contribution of primary BrC about 20% but enhanced contribution of secondary
23 BrC by 30%, implying the concurrent whitening and darkening of BrC. This provides field evidence that the photochemically
24 produced secondary nitrogen-containing OA can considerably compensate some bleaching effect on the primary BrC, hereby
25 causing radiative impacts.

26 1. Introduction

27 Atmospheric absorbing organic aerosol (OA), known as brown carbon (BrC), is important contributor to anthropogenic
28 absorption besides black carbon (BC) (Laskin et al., 2015; Liu et al., 2020), particularly at shorter visible wavelengths (Bahadur
29 et al., 2012). Due to complex compositions of OA, the primary sources and subsequent evolution of BrC in the atmosphere
30 remains to be explicitly understood and causes uncertainties in evaluating the radiative impacts of BrC (Liu et al., 2020).
31 The chromophores of BrC are mainly aromatic compounds associated with certain functional groups (Liu et al., 2015c).
32 Particularly, compounds containing nitro, nitrated or other forms of nitrogen-containing functional groups are more absorbing
33 (Nakayama et al., 2013; Jacobson, 1999). It is well established that primary OA, especially from biomass burning, contains a
34 large fraction of BrC (Andreae and Crutzen, 1997; Rizzo et al., 2013; Bond, 2001). These primary BrC had a range of
35 absorptivity, which was found to be controlled by burning phases, with OA co-emitting with BC (the flaming phase) exhibiting
36 a higher absorptivity than OA-dominated smoldering phase (Liu et al., 2021). BrC can experience reactions with atmospheric
37 oxidants after emission. Previous studies (Satish et al., 2017; Satish and Rastogi, 2019) found nitrogenous compounds from
38 biomass burning were responsible for brown carbon over South Asia and the chromophores were photobleached in the
39 afternoon. Numerous field and laboratory studies found the decrease of BrC absorptivity due to photobleaching on
40 chromophores, with lifetime ranging from a few hours (Zhao et al., 2015; Liu et al., 2021) to a few days (Forrister et al., 2015),
41 which may depend on the concentration of ambient hydroxyl radical (Wang et al., 2014), also influenced by relative humidity
42 and particle volatility (Schnitzler et al., 2020). The absorptivity of BrC could be also enhanced due to addition of functional
43 groups by forming conjugated structure with aromatics. This was supported by a number of laboratory studies that BrC
44 absorptivity could be enhanced when forming nitrogen-containing organic compounds, such as the formation of nitro-
45 aromatics when aromatics reacted with NO_x (Nakayama et al., 2013), or produced organic amine after reacting with ammonia
46 (Updyke et al., 2012). The enhancement of BrC absorptivity could occur either through nitration of existing chromophores, or
47 formation of new secondary organic aerosol (SOA) chromophores through gas-phase oxidation.

48 The above findings mean the enhancement or bleaching of BrC absorptivity via photooxidation will coexist. The time scale
49 between both competing processes will ultimately determine the lifetime of BrC in the atmosphere. However, both processes
50 have been rarely investigated in the field to explicitly determine the BrC components which principally determine the
51 respective enhancement or decrease of its absorptivity, particularly in regions influenced by combined anthropogenic sources.
52 In this study, by measurements using multiple-wavelength absorption and microphysical properties of BC in a sub-urban region,
53 the absorption of BC, primary and secondary BrC was discriminated. In conjunction with source attribution via OA mass
54 spectra, we are able to link the segregated absorption with certain sources and investigate their primary information and
55 subsequent evolution. The competition between photobleaching and secondary formation of BrC was investigated in real world.

56 2. Experimental and instrumentation

57 2.1 Site description and meteorology

58 The experiment was conducted during springtime at the Beijing Cloud Laboratory and Observational Utilities Deployment
59 Base (117.12°E, 40.14°N), which is located in the northeast suburban area in Beijing (Fig S1a). The site is surrounded by the
60 northwest mountain ridge, without significant local primary anthropogenic emissions (Hu et al., 2021). The 72-h backward
61 trajectories with every 3 hours initializing from the site are analyzed by the HYSPLIT model (Draxier and Hess, 1998) using
62 the 3-hourly 1°×1° meteorological field from the GDAS reanalysis product. The obtained backward trajectories were further
63 clustered to group the similar transport pathways (Makra et al., 2011). The meteorological parameters, including the
64 temperature (T), ambient relative humidity (RH), wind speed (WS) and wind direction (WD) were measured by a monitoring
65 station on the site.

66 2.2 Measurements of BC microphysics and absorption coefficient

67 In this study, the ambient aerosols were sampled by a large-flow (1.05 m³ min⁻¹) air particle sampler (TH-1000C II) with a
68 PM_{2.5} impactor (BGI SCC 1.829) and dried by a silica drier before measurement. The single particle soot photometer (SP2,
69 DMT., USA) used continuous laser at λ=1064nm to incandesce light-absorbing aerosols (such as BC) for irradiating detectable
70 visible light. The incandescence signal was used to measure the refractory black carbon (rBC) mass. The SP2 incandescence
71 signal was calibrated using the Aquadag standard (Acheson Inc., USA), and a factor of 0.75 was applied to correct for ambient
72 BC (Laborde et al., 2012). The scattering signal was calibrated by monodispersed polystyrene latex spheres (PSL). The BC
73 core diameter (D_c) was calculated from the measured BC mass by assuming a BC density of 1.8 g cm⁻³ (Bond and Bergstrom,
74 2006). The leading edge only (LEO) method was applied to reconstruct the scattering signal of BC, which was used to
75 determine the coated particle diameter (D_p) by a Mie-lookup table with the inputs of scattering and incandescence signal of
76 each BC particle (Liu et al., 2014; Taylor et al., 2015). The mass median diameter (MMD) is derived from the D_c distribution,
77 which is determined as below and above MMD the rBC mass concentration is equal (Liu et al., 2019a). The bulk coating
78 thickness (D_p/D_c) is calculated as the cubic root of ratio of the total coated BC volume divided by the total volume of rBC.
79 The mass absorption cross section (MAC) (in m² g⁻¹) of each BC particle can be calculated using the measured coated and
80 uncoated BC sizes by applying the Mie core-shell calculation. The absorption coefficient of BC at certain wavelength, σ_{abs,BC}
81 (λ) is determined by multiplying the calculated MAC and rBC mass concentration at each size:

$$82 \sigma_{\text{abs,BC}}(\lambda) = \sum_i \text{MAC}(\lambda, D_{p,i}, D_{c,i}) m(\log D_{c,i}) \Delta \log D_{c,i} \quad (1)$$

83 where m(log D_{c,i}) denotes the BC mass concentration at each logarithmic bin of D_c. The SP2 measurement at λ=1064nm longer
84 than mostly populated BC size means the derived coatings and subsequent calculation of MAC is relatively independent of
85 particle shape within uncertainty of 21% (Liu et al., 2014; Hu et al., 2021).

86 The absorption coefficients at wavelengths λ= 375, 470, 528, 635 and 880 nm were measured by a Micro-Aethalometer
87 (MA200, Aethlabs, San Francisco, CA, USA). Aerosol particles were collected on filter tapes, on which the light attenuation
88 was measured continuously with a time resolution of 30 s. The loading effect of filters was automatically corrected by

89 measuring attenuation at two different sampling flow rates on two spots in parallel (Drinovec et al., 2015). Moreover, a multi-
 90 scattering correction factor (C-value) of 3.5, 3.2 and 2.4 at the wavelengths 370 nm, 528 nm and 880 nm, respectively were
 91 utilized to correct attenuation for the multiple light scattering effect. It was obtained by comparing the absorption coefficient
 92 with a photoacoustic soot spectrometer (PASS-3, DMT) (Hu et al., 2021).

93 2.3 Attribution of primary and secondary BrC absorption coefficient

94 The absorption coefficient of BC at different λ is calculated using the measured uncoated core and coated size as mentioned
 95 above. The absorption coefficient of total BrC is obtained by subtracting the BC absorption coefficient from the total absorption
 96 at certain wavelength, expressed as:

$$97 \sigma_{\text{abs, BrC}}(\lambda) = \sigma_{\text{abs, total}}(\lambda) - \sigma_{\text{abs, BC}}(\lambda) \quad (2)$$

98 where the absorption coefficient of BC ($\sigma_{\text{abs, BC}}$) is obtained from the SP2 measurement, $\sigma_{\text{abs, total}}(\lambda)$ is the total light absorption
 99 of aerosols measured by the MA200. The absorption coefficient of secondary BrC, the absorption not contributed by primary
 100 sources, is obtained by subtracting the absorption of all primary sources from the total absorption (Crilley et al., 2015),
 101 expressed as:

$$102 \sigma_{\text{abs, secBrC}}(\lambda) = \sigma_{\text{abs, total}}(\lambda) - \sigma_{\text{abs, pri}}(\lambda) \quad (3)$$

103 where $\sigma_{\text{abs, pri}}(\lambda)$ is the light absorption from primary sources. Here an assumption is made that light absorption from primary
 104 aerosols is all from combustion sources, and these sources necessarily contain BC (Wang et al., 2018). Therefore, the total
 105 absorption from primary sources can be obtained by scaling a factor from the mass concentration of BC, expressed as:

$$106 \sigma_{\text{abs, pri}}(\lambda) = \left(\frac{\sigma_{\text{abs, total}}}{[\text{rBC}]} \right)_{\text{pri}} \cdot [\text{rBC}] \quad (4)$$

107 where [rBC] is the mass concentration of rBC measured by the SP2, $\left(\frac{\sigma_{\text{abs, total}}}{[\text{rBC}]} \right)_{\text{pri}}$ is the scaling factor to derive the
 108 absorption of primary combustion sources from [rBC]. This factor is obtained using the minimum R-squared (MRS) approach
 109 (Wu and Yu, 2016), by adjusting the factor until a minimum correlation between $\sigma_{\text{abs, secBrC}}$ and [rBC] is reached because the
 110 absorption from secondary sources are least likely to covary with that from primary sources (Wang et al., 2019a). This method
 111 has been used in urban and sub-urban environment to obtain the primary BrC associated with combustion sources. Different
 112 sources may exhibit different ratios of $\left(\frac{\sigma_{\text{abs, total}}}{[\text{rBC}]} \right)_{\text{pri}}$, however there were no sporadic pollution events during the experimental
 113 period, uniform sources are therefore considered, and this ratio tends to represent a mean for the experiment. Being different
 114 from previous studies, an auxiliary characterization of rBC mass measured by the SP2 is used here to avoid the possible
 115 interference from absorption measured by the same instrument. The $\left(\frac{\sigma_{\text{abs, total}}}{[\text{rBC}]} \right)_{\text{pri}}$ ratio at $\lambda=375$ nm, 470 nm, 528 nm, 635
 116 nm and 880 nm is calculated to be 20.7, 17.0, 14.4, 11.7 and 5, respectively (Fig. S2), which falls within the reported values
 117 from previous studies 11-50 (Zhang et al., 2020; Wang et al., 2019a). This scenario assumes a relatively consistent absorption
 118

119 relative to BC mass concentration from sources during experiment. This however may not include some sporadic events when
120 sources with distinct OA or BC mass fraction may be introduced and alter the single $\left(\frac{\sigma_{abs,total}}{[rBC]_{pri}}\right)$ ratio. The $\sigma_{abs,secBrC}$
121 therefore represents the overall mean value during the experimental period but this ratio will vary with seasons and locations.
122 The σ_{abs} of primary BrC can then be calculated as:

$$123 \sigma_{abs,priBrC}(\lambda) = \sigma_{abs,BrC}(\lambda) - \sigma_{abs,secBrC}(\lambda) \quad (5)$$

124 where $\sigma_{abs,BrC}$ and $\sigma_{abs,secBrC}$ is calculated from Equation (2) and (3), respectively. When evaluated the contribution of
125 photooxidation to the absorption coefficient, the absorption coefficient during photooxidation (12:00-17:00) was divided by
126 the respective average absorption coefficients of primary and secondary BrC.

127 2.4 Composition measurement

128 The mass concentration and chemical composition of non-refractory sub-micron PM (NR-PM₁) including organic aerosols
129 (OA), nitrate (NO₃⁻), sulfate (SO₄²⁻), chloride (Cl⁻) and ammonium (NH₄⁺) were determined with a High-Resolution Time-of-
130 Flight Aerosol Mass Spectrometer (HR-ToF-AMS, Aerodyne Research Inc., USA). The setup, operation, and calibration
131 procedures of the AMS have been described elsewhere (Canagaratna et al., 2007). During this field observation, the AMS was
132 operated in V-mode for the quantification of mass concentrations. The composition-dependent collection efficiencies were
133 applied (Middlebrook et al., 2012), and the ionization efficiency was calibrated using 300 nm pure ammonium nitrate (Jayne
134 et al., 2000). Elemental ratios of OA including oxygen-to-carbon (O/C), hydrogen-to-carbon (H/C) and nitrogen-to-carbon
135 (N/C) were determined to the improved-ambient method (Canagaratna et al., 2015).

136 Positive Matrix Factorization (PMF) (Paatero and Tapper, 1994) was performed on the inorganic and organic high-resolution
137 mass spectra to distinguish OA components from different sources (Zhang et al., 2011; Ulbrich et al., 2009; Decarlo et al.,
138 2010). The mass spectra of the combined matrix for m/z < 120 were excluded in PMF analysis. Five OA factors were identified.
139 The diagnostics of PMF is summarized in Text S1 and Fig. S6.

140 2.5 Offline Fourier transform infrared spectrometer (FTIR) analysis

141 Particulate Matter (PM) samples were collected once a day onto prebaked (600°C, 4h) quartz fiber filters (Whatman, QMA,
142 USA) using a large-flow (1.05 m³ min⁻¹) air particle sampler (TH-1000C II). The collected filter samples were stored in the
143 refrigerator at -20°C before analysis. The infrared spectra of collected samples were measured by a Fourier transform infrared
144 spectrometer (FTIR, Thermo Scientific, USA) equipped with an iD5 attenuated total reflectance accessory (diamond crystal)
145 to quantify the chemical functional groups over the wavenumbers range of 550-4000 cm⁻¹ with a resolution of 0.5 cm⁻¹. The
146 NO and NO₂ symmetric stretch in the FTIR spectra can characterize the functional groups associated with nitrogen-containing
147 organics (Coury and Dillner, 2008). Fig. S3 shows typical examples of FTIR spectra and the assigned functional groups for
148 the three pollution levels during experiment. The peak at 1110 cm⁻¹ corresponds to the background of the quartz fiber filter
149 overlapped with some X-H bending vibrations, which is subtracted for the following analysis. The characteristic organic nitrate

150 spectra appear at wavenumbers 860 cm^{-1} (NO symmetric stretch), 1280 cm^{-1} (NO_2 symmetric stretch) and $1630\text{-}1640\text{ cm}^{-1}$
151 (NO_2 asymmetric stretch) (Bruns et al., 2010). After baseline calibration, The FTIR peaks of 1630 cm^{-1} and 860 cm^{-1} are
152 integrated the absorption areas above the baseline. The summed integrated area of -NO and - NO_2 are hereby used to indicate
153 the nitrogen-containing organics. There was no discernable peak of carbonyl group for our infrared spectrum, and the peak of
154 OH at 2500 cm^{-1} - 3400 cm^{-1} for the carboxylic acid is not discernable neither, thus the influence of ketone and carboxylic acid
155 may be of less importance for our dataset.

156 3. Results and Discussion

157 3.1 Source attributed OA

158 The overview results are shown in Fig. S1. The organics dominated the aerosol compositions for most time, but occasionally
159 nitrate was the most abundant component (Fig. S1g). Note that the nitrate here may also include components containing in
160 organics besides ammonium nitrate. Backward trajectories (Fig. S1a-d) showed that the most abundant PM_{10} concentration was
161 associated with air masses transported in shorter distance from southern regions (C1), but the longer and faster northerly
162 transported air mass from cleaner north (C2) could dilute the concentrations.

163 The resolved OA factors by the PMF analysis are shown in Fig. 1, including the mass spectra, time series and diurnal profiles
164 of each PMF factor with corresponded external and internal tracers. Three primary OA (POA) were identified as hydrocarbon-
165 like OA (HOA), cooking-related OA (COA), biomass burning OA (BBOA), with O/C of 0.31, 0.18 and 0.39 respectively.
166 These POA had considerable fraction of hydrocarbon fragments (C_xH_y), indicating their less aged status. The HOA profile was
167 characterized by higher contributions of aliphatic hydrocarbons and has dominated ion tracers such as m/z 41 (C_3H_5^+), 43
168 (C_3H_7^+), 55 (C_4H_7^+) and 57 (C_4H_9^+). The HOA concentration correlated with BC ($r=0.62$), which emits from traffic emissions.
169 The diurnal variation exhibited strong morning and afternoon rush-hour peaks of mass concentration. This factor was consistent
170 with the mass spectra of previously measured HOA from on-road vehicle emissions in urban cities (Zhang et al., 2005; Aiken
171 et al., 2009; Sun et al., 2016; Hu et al., 2017), which has m/z peaks characteristic of hydrocarbon fragments in series of $\text{C}_n\text{H}_{2n+1}^+$
172 and $\text{C}_n\text{H}_{2n-1}^+$. The mass spectrum of HOA shows overall similarity to those of primary OA emitted from gasoline and diesel
173 combustion sources ($r=0.68$) (Elser et al., 2016).

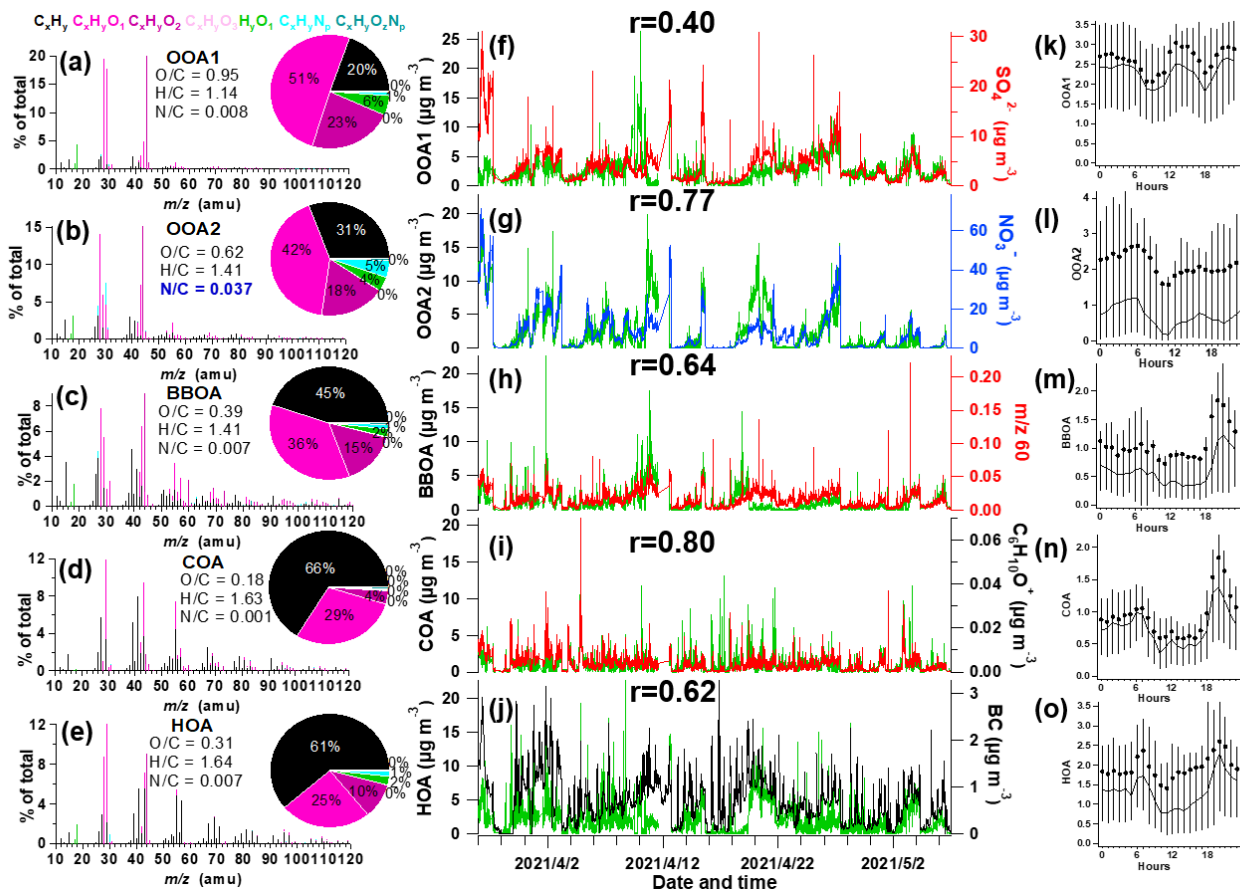
174 The OA from cooking sources (COA) is also characterized by prominent hydrocarbon ion series, however, with higher signal
175 at $\text{C}_n\text{H}_{2n-1}^+$ than $\text{C}_n\text{H}_{2n+1}^+$. COA had apparent fragments of both C_4H_9^+ and $\text{C}_3\text{H}_3\text{O}^+$, and has a higher ratio of $\text{C}_3\text{H}_3\text{O}^+/\text{C}_3\text{H}_5\text{O}^+$
176 (3.1), $\text{C}_4\text{H}_7^+/\text{C}_4\text{H}_9^+$ (2.2) than HOA (0.9–1.1), with cooking-related fragments of $\text{C}_5\text{H}_8\text{O}^+$ (m/z 84), $\text{C}_6\text{H}_{10}\text{O}^+$ (m/z 98) and
177 $\text{C}_7\text{H}_{12}\text{O}^+$ (m/z 112) (Sun et al., 2011b; Mohr et al., 2012). The COA shows overall similar spectral pattern to the reference
178 spectra of COA ($r=0.92$) (Elser et al., 2016). Its minor peak at noon and larger peak in the evening (Fig. 11) also corresponded
179 with the lunch and dinner time respectively. There was only a minor peak at noon for COA, which may be due to the sub-urban
180 nature of the site where the major aerosols from cooking sources may have been processed and lost the signature near source.

181 The feature of this factor was also observed in sub-urban environment (Huang et al., 2021).

182 The BBOA factor was identified based on the prominent signals of m/z 60 ($C_2H_4O_2^+$) and 73($C_3H_5O_2^+$), which are known
183 fragments of levoglucosan (Cubison et al., 2011). And BBOA also correlated with potassium (K^+ , $r = 0.80$), which are indicator
184 of biomass burning (Pachon et al., 2013; Brown et al., 2016). The m/z 60 and 73 together with a unique diurnal variation have
185 been shown to be a robust marker for the presence of aerosols from biomass burning emissions in many urban locations (Sun
186 et al., 2016). The BBOA shows very similar mass spectral patterns to previously reported reference spectra of biomass burning
187 ($r=0.94$) (Elser et al., 2016). The BBOA factor that was identified in spring accounted for 12.8% of the total OA in Beijing,
188 similar to previous reports (Hu et al., 2017). Biomass (Cheng et al., 2013) and solid fuel burning emissions (Sun et al., 2014)
189 have been widely observed to importantly contribute to the primary OA in this region. This off-road combustion source was
190 particularly abundant during wintertime for residential heating activities (Shen et al., 2019; Yang et al., 2018; Liu et al., 2016),
191 while boiler for industry use (mostly using coal as fuel) was in operation throughout the year (Liu et al., 2015b). During the
192 springtime of the experiment, the residential heating activities dropped due to increased ambient temperature thus the BBOA
193 may be mainly contributed by the industry sector.

194 Two types of oxygenated organic aerosols (OOA) were identified, in moderate (OOA2, O/C=0.62) and high oxidation state
195 (OOA1, O/C=0.95), respectively, which is very similar to the spectra of OOA factors resolved in other cities (Hayes et al.,
196 2013; Ulbrich et al., 2009). The average mass spectrum of OOA2 in this study is characterized by m/z 29 (mainly CHO^+), 43
197 (mainly $C_2H_3O^+$) and m/z 44 (CO_2^+), similar to the semi-volatile OOA spectrum identified in other locations (Sun et al., 2011a;
198 Zhou et al., 2016). On average, OOA2 accounts for 42% and 18% of $C_xH_yO^+$ and $C_xH_yO_2^+$ ions, respectively (Fig. 1b). These
199 results clearly indicate that OOA2 was primarily composed of less oxygenated, possibly freshly oxidized organics. Notably,
200 OOA2 had a substantially higher N/C than other factors (N/C=0.037), and had highest correlation with nitrate ($r=0.77$) and
201 with $C_xH_yN_z$ and $C_xH_yN_zO_p$ fragments ($r=0.83$). This factor therefore tends to largely result from nitrogen-containing OA and
202 its elevation at night may be also associated with dark oxidation by nitrate radical.

203 The mass spectrum of OOA1, which was characterized by a dominant peak at m/z 44 (mainly CO_2^+), a highest O/C (0.95). On
204 average, OOA1 contributes 51% of the $C_xH_yO^+$ signal and 23% of the $C_xH_yO_2^+$ signal (Fig. 1a). OOA1 showed particularly
205 high correlation with sulfate ($r=0.40$) because of their similar volatilities (Huffman et al., 2009; Jimenez et al., 2009). The
206 slight enhancement at noon for OOA1 (also for OOA2) soon after morning rush-hour indicated the likely rapid formation of
207 SOA through photooxidation. This significantly higher mean OOA2 than median value in the diurnal pattern indicated that
208 this OA type was largely associated with pollution events. Both OOA1 and OOA2 showed nighttime peak maybe due to
209 reduced boundary layer.

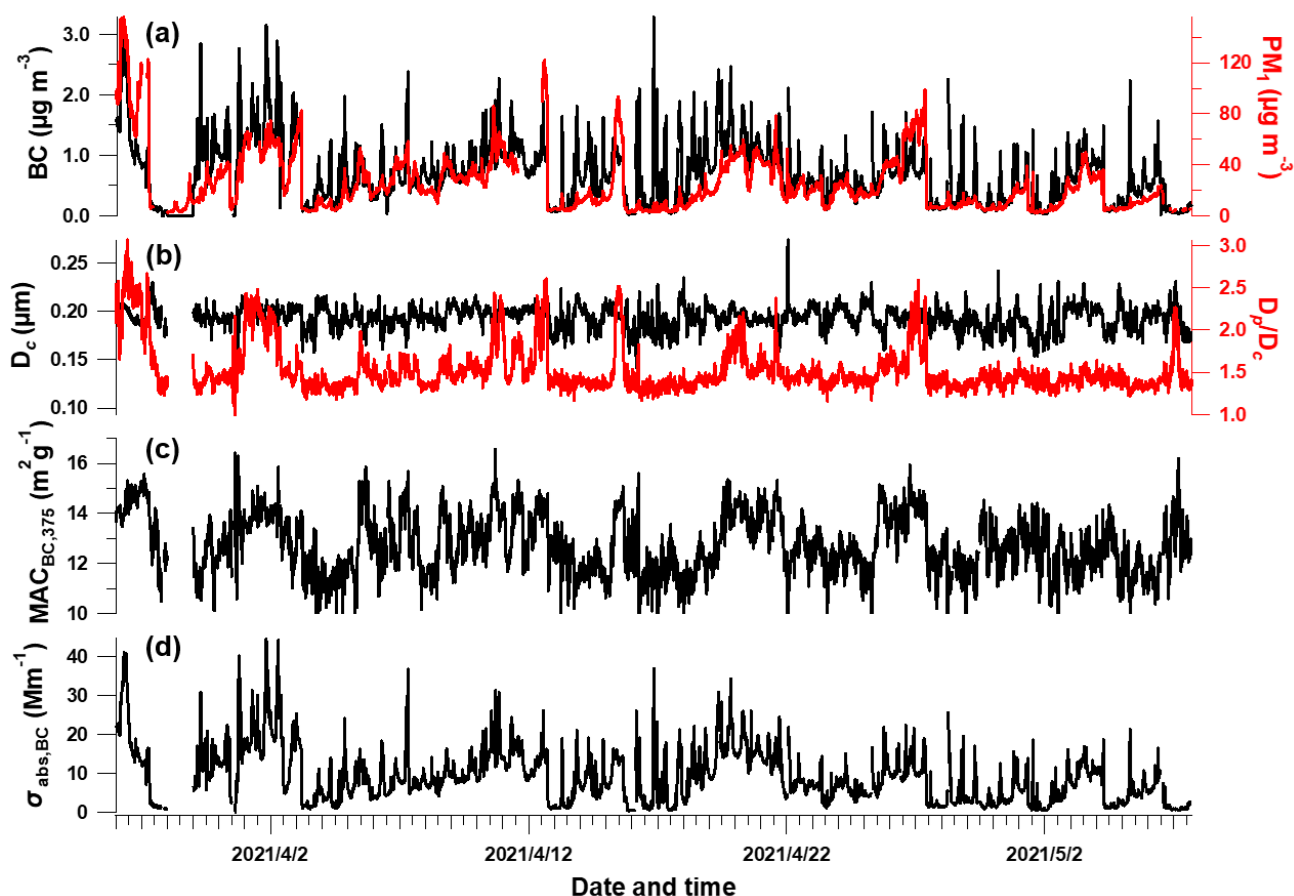


210
 211 **Figure 1. Information of source-apportioned organic aerosols by the PMF analysis. Mass spectra of (a) oxygenated OA1 (OOA1), (b)**
 212 **oxygenated OA2 (OOA2), (c) biomass burning OA (BBOA), (d) cooking-related OA (COA), (e) hydrocarbon-like OA (HOA), (f-j)**
 213 **Temporal variations of each PMF factor and the corresponding marker species. (k-o) Diurnal profiles of each factor. The lines, dots**
 214 **and whiskers denote the median, mean and the 25th/75th percentiles at each hour respectively.**

215 3.2 Segregated aerosol absorption

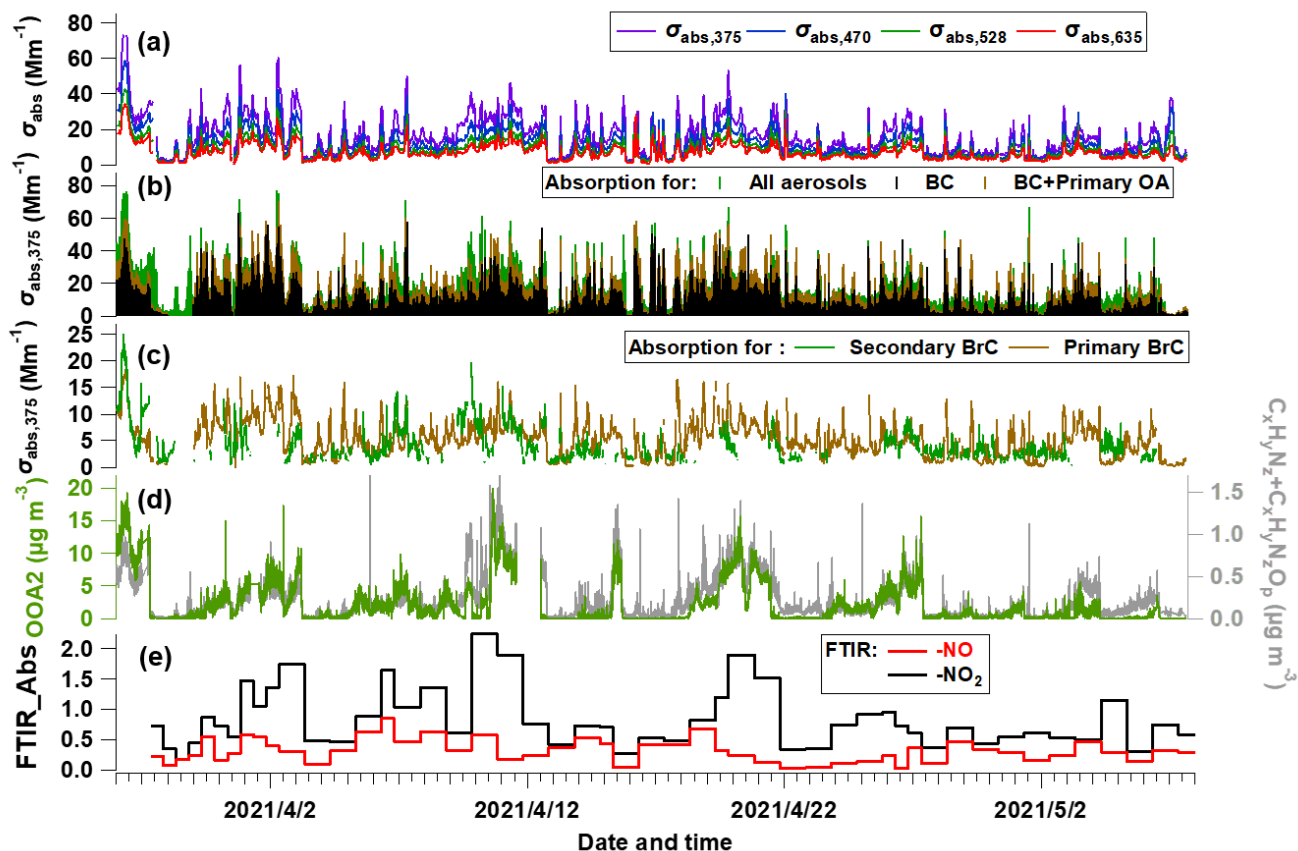
216 Fig. 2 shows the time series of BC properties, including the BC mass concentration, D_p/D_c , D_c , MAC and light absorption
 217 coefficient of BC (section 2.2). The MMD of BC core varied between 93 – 274 nm which may correspond to the source-
 218 specific information (Liu et al., 2019b) or coagulation process during ageing. The coating of BC (indicated by D_p/D_c) showed
 219 sporadic enhancement which was closely associated with enhanced PM concentration (Fig. 2a). This was consistent with
 220 previous studies that high coatings of BC occurred during heavier pollution due to the enhanced secondary formation of
 221 condensable materials to particle phase (Ding et al., 2019; Zhang et al., 2018). This clearly indicates the variation of mixing
 222 state of BC and this will potentially influence its MAC and absorption Ångström exponent (AAE) (Liu et al., 2015a). It will
 223 introduce considerable uncertainties to use constant MAC or AAE to derive the absorption coefficient of BC at multiple
 224 wavelengths. The MAC estimated using the measured BC core size and coatings (Fig. 2c) is thus used to derive the $\sigma_{\text{abs,BC}}$
 225 (section 2.2, shown in Fig. 2d). The $\sigma_{\text{abs,BC}}$ was $9.1 \pm 7.3 \text{ Mm}^{-1}$ during experimental period. MAC of BC at $\lambda=375\text{nm}$ showed to

226 be at $8.4 - 16.6 \text{ m}^2 \text{ g}^{-1}$ with enhanced absorption when high coatings.



227
228 **Figure 2. Temporal evolution of BC-related properties. (a) rBC and PM_{10} mass concentration, (b) BC core diameter and bulk coating**
229 **thickness (D_p/D_c), (c) calculated mass absorption cross section (MAC) at $\lambda=375\text{nm}$, (d) absorption coefficient of BC.**

230 Using the method above, the total ($\sigma_{\text{abs,total}}$) and attributed absorption of BC ($\sigma_{\text{abs,BC}}$), primary ($\sigma_{\text{abs,priBrC}}$) and secondary BrC
231 ($\sigma_{\text{abs,secBrC}}$) at $\lambda=375\text{nm}$ are shown in Fig. 3a-c. In Fig. 3b, the brown and green shades above the adjacent tracer indicate the
232 absorption coefficient of primary and secondary BrC, respectively. Fig. 3c shows that the absorption coefficient of primary
233 BrC was higher than secondary BrC for most time, but for certain periods they were equivalent or secondary BrC occasionally
234 exceeds primary BrC. The mean contribution of absorption coefficient for BC, primary BrC and secondary BrC is 51%, 27%
235 and 22% in this study. The tracers associated with nitrogen-containing organics, such as OOA2 (with highest N/C), $\text{C}_x\text{H}_y\text{N}_z$
236 and $\text{C}_x\text{H}_y\text{N}_z\text{O}_p$ fragments, and the FTIR measured $-\text{NO} + -\text{NO}_2$, are also shown in Fig. 3d-e.



237
 238 **Figure 3. Temporal evolution of segregated absorbing properties. (a) Absorbing coefficients (σ_{abs}) at multiple wavelengths measured**
 239 **by the aethalometer, (b) σ_{abs} at $\lambda=375\text{nm}$ ($\sigma_{\text{abs},375}$) for all aerosols, primary OA and BC, (c) $\sigma_{\text{abs},375}$ for primary BrC and secondary**
 240 **BrC. (d) mass concentration of OOA2 and the $\text{C}_x\text{H}_y\text{N}_z$ and $\text{C}_x\text{H}_y\text{N}_z\text{O}_p$ fragments measured by the AMS. (e) FTIR-measured**
 241 **absorption of -NO and -NO₂ bonds.**

242 3.3 Source attribution of BrC absorption

243 A multiple linear regression (MLR) analysis is performed to apportion the absorption coefficient of BrC with the PMF
 244 attributed OA factors, expressed as:

$$245 \sigma_{\text{abs,BrC}} = a_0 + a_1 \cdot [\text{OOA1}] + a_2 \cdot [\text{OOA2}] + a_3 \cdot [\text{BBOA}] + a_4 \cdot [\text{COA}] + a_5 \cdot [\text{HOA}] \quad (6)$$

246 where a_1 to a_5 represents the regression coefficients for each factor. The contribution of each source-specific OA factor to
 247 $\sigma_{\text{abs,BrC}}$ can be obtained. This analysis is performed for the total BrC, primary and secondary BrC respectively. The results are
 248 shown in Table 1. MLR on the total BrC shows high correlation ($r > 0.4$) with the factors of HOA, BBOA and OOA2, suggesting
 249 the potential importance of the primary biomass burning and traffic source along with OOA2 in governing absorption of BrC.
 250 MLR analysis on the primary BrC distinguishes its substantial correlation with BBOA ($r = 0.40$) and HOA ($r = 0.46$), while MRL
 251 on the secondary BrC has a high correlation with OOA2 only ($r = 0.44$). The MRL analysis links the apportioned absorption of
 252 physical properties with source-attributed chemical compositions, therefore validating and identifying the sources of primary

254 **Table 1. Results of the multilinear regression analysis (MLR) between $\sigma_{\text{abs},375}$ and the five PMF-resolved OA factors, with $\sigma_{\text{abs},375}$ of**
 255 **total BrC, primary and secondary BrC as dependent, respectively. All regression coefficients have passed the significance test with**
 256 **$p < 0.01$. Partial correlations above 0.4 are marked in red. Since negative values appear when the COA participates, which is thus not**
 257 **included in the final regression but the values using COA factor are shown in brackets.**

Dependent	$\sigma_{\text{abs},\text{BrC}}$		$\sigma_{\text{abs},\text{pri BrC}}$		$\sigma_{\text{abs},\text{sec BrC}}$	
	Regression coefficient	Partial correlation	Regression coefficient	Partial correlation	Regression coefficient	Partial correlation
Constant	2.26		1.67		1.47 (1.52)	
OOA1	0.57	0.23	0.04	0.02	0.46(0.46)	0.24 (0.24)
OOA2	1.22	0.53	0.37	0.25	0.74 (0.74)	0.44 (0.44)
BBOA	2.59	0.46	1.22	0.40	1.14 (1.18)	0.29 (0.29)
COA	1.30	0.22	1.45	0.36	/ (-0.25)	/ (-0.05)
HOA	1.70	0.47	1.17	0.46	0.49 (0.52)	0.20 (0.21)
R ²		0.77		0.63		0.55 (0.55)

258 Importantly, an oxygenated secondary OA factor (OOA2) is identified to significantly contribute to the secondary BrC. This
 259 OOA has a moderate O/C (0.62) and a highest N/C of 0.037 among all factors. The high N/C means this factor contains the
 260 most abundant nitrogen-containing fragments, implied as its high correlation with the $\text{C}_x\text{H}_y\text{N}_z$ and $\text{C}_x\text{H}_y\text{N}_z\text{O}_p$ fragments ($r=0.83$,
 261 Fig. 3d) and with the FTIR absorption for -NO₂ and -NO bonds ($r=0.69$, Fig. S4). The -NO bond is mostly related to the
 262 organic nitrates (RONO₂), and -NO₂ peak could result from both organic nitrates and nitro-organics (Bruns et al., 2010). There
 263 is no discernable peak for organic amines. These all consistently imply that the OOA2 factor contained substantial fraction of
 264 nitrogen-containing organics, and these compounds have contributed to the absorption of secondary BrC.

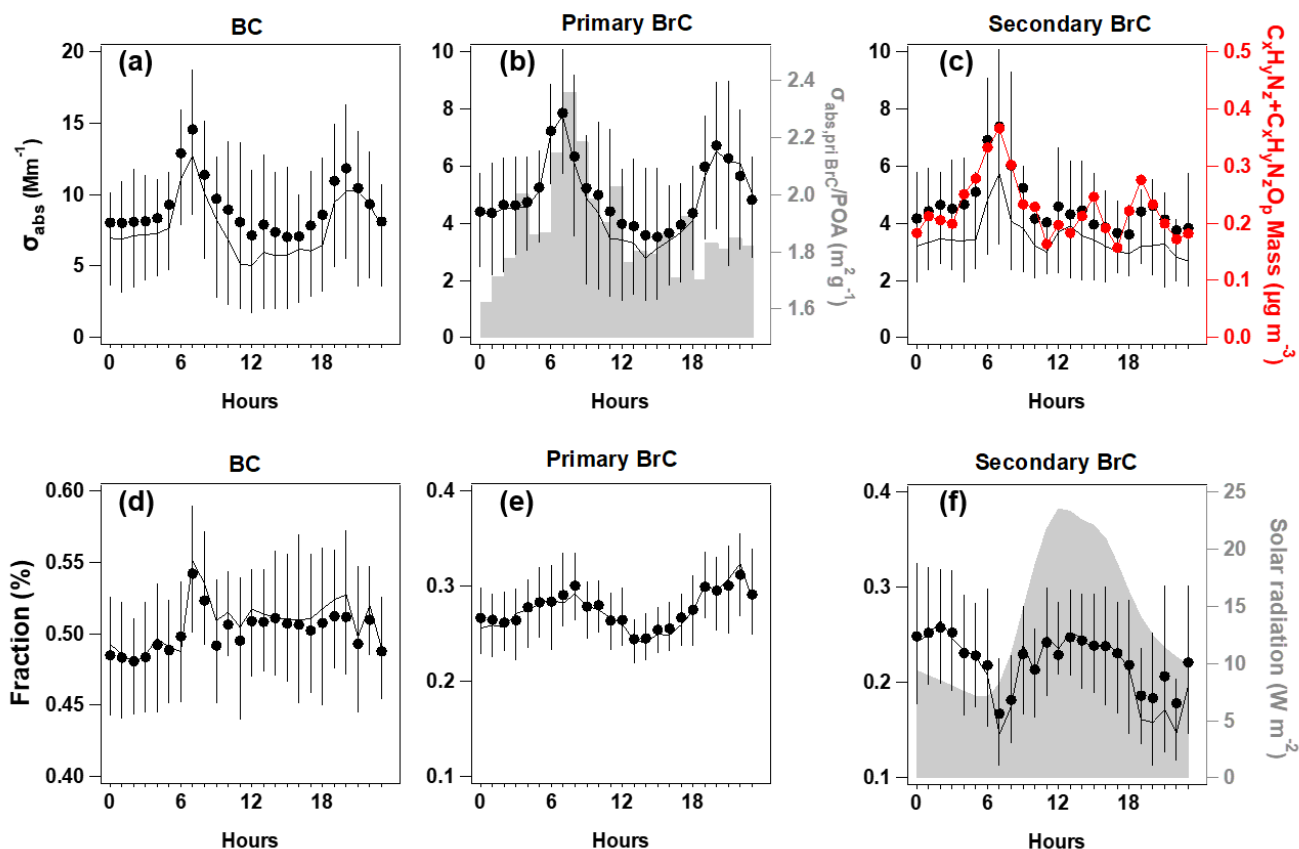
265 3.4 Simultaneous whitening and darkening process of BrC

266 The diurnal variation of $\sigma_{\text{abs},375}$ for BC and primary BrC and their fractions showed consistent morning rush-hour peaks at
 267 6:00-8:00 and the night-time enhancement due to reduced boundary layer (Fig. 4a-b). This was in line with the morning peak
 268 of HOA and night peak of BBOA. The traffic source in this region, in particular the diesel vehicles, was reported to emit
 269 considerable OA with certain chromophores, such as aromatics (Yao et al., 2015) and heterocyclic organic compounds (Gentner
 270 et al., 2017; Schuetzle, 1983). In the morning rush-hour, BC and primary BrC accounted for 51±4% and 29±4% in the total
 271 $\sigma_{\text{abs},375}$ respectively, with the remaining 20±2% classified as secondary BrC. The morning peak coinciding with the primary
 272 BrC may result from the rapid formation of BrC from sources when emitted gases condensed and formed aerosols. These may
 273 lead to high cooccurrence between primary and secondary BrC. Previous studies in urban environment also observed

274 concurrent peaks of primary and secondary BrC, which usually occurred at morning rush hour (Zhang et al., 2020). The night
275 had contributions from BC and primary BrC at $50\pm 2\%$ and $30\pm 3\%$ respectively, with $20\pm 3\%$ as secondary BrC. Fig. 4b showed
276 the decrease of primary BrC absorption tended to be more rapid than the HOA and BBOA mass (even a slight increase for
277 HOA Fig. 1m and Fig. 1o), leading to decreased absorption coefficient per unit mass of primary BrC (shade in Fig. 4b), which
278 indicates the photobleaching process. In this context, a recent chamber study reported that the primary BrC from biomass
279 burning plumes could be bleached to half of the initial absorptivity in 2-3 hours (Liu et al., 2021).

280 Besides the morning rush-hour peak, there was an early afternoon peak for the absorption coefficient of secondary BrC,
281 prevailing the dilution effect of daytime boundary layer (Fig. 4c-S5). The night and morning peak of OOA2 and the morning
282 peak of $\sigma_{\text{abs,secBrC}}$ may result from primarily emitted moderately oxygenated OA, which was reported from some diesel sources
283 (Dewitt et al., 2015; Gentner et al., 2012). The fraction of secondary BrC thus had a pronounced early afternoon peak soon
284 after the peak solar radiation (Fig. 4f) and a peak after midnight soon after the nighttime peak of primary BrC (Fig. 4e). Fig
285 4e-f shows the photooxidation led to an enhanced contribution of secondary BrC by 30% but reduced contribution of primary
286 BrC about 20%. This shift of peaking time from primary to secondary BrC demonstrates the likely process of SOA formation
287 from gases, and these SOA compounds containing nitrogen (i.e., the OOA2) considerably contributed to the light absorption.
288 This ageing or oxidation likely occurred through photooxidation during early afternoon and aqueous processes (high RH
289 conditions prevail during nighttime) during nighttime. The oxidized volatile organic compounds (VOCs) with nitrogen
290 chemistry involved could condense to produce additional mass in particle phase (Ehn et al., 2014; Finewax et al., 2018). Due
291 to the high NO_x emission, photooxidation of traffic VOCs may have largely involved nitrogen chemistry. Previous studies
292 found the NO_x -involved SOA could produce considerable chromophores (Lin et al., 2015; Siemens et al., 2022), such as the
293 traffic VOCs may produce SOA in a time scale of hours, containing nitro-aromatics (Wang et al., 2019b; Keyte et al., 2016).
294 The daytime formation of organic nitrate may follow the gas-phase photooxidation mechanism, in which the excess NO could
295 add to the peroxy radical to produce organic nitrate (Liebmann et al., 2019). The nighttime chemistry involving NO_3 radical
296 through the oxidation of NO_2 by O_3 , contributed to the important formation of organic nitrate by initializing the production of
297 nitrooxy peroxy radicals (Ng et al., 2008; Rollins et al., 2012). Laboratory studies (Nakayama et al., 2013; Liu et al., 2015c)
298 also widely observed the rapid production of nitrogen-containing OA involving NO_x chemistry could contribute to light
299 absorption of aerosols.

300 Overall, by apportioning the absorption of primary and secondary BrC, we found the photooxidation led to an enhanced
301 contribution of secondary BrC by 30% but reduced contribution of primary BrC about 20% in the semi-urban environment.
302 This revealed that the whitening and darkening of BrC occurred simultaneously, and the secondary BrC produced by
303 photooxidation may compensate some bleaching effect of primary BrC. The dominance of both competing processes may
304 depend on the timescale and altitude in the atmosphere. For example, the enhanced BrC fraction observed above the planetary
305 boundary layer may be explained by the enhanced secondary BrC (Tian et al., 2020), while further ageing may bleach the
306 produced chromophores of these SOA.



307
 308 **Figure 4. Diurnal variations of absorption coefficient at $\lambda=375\text{nm}$ ($\sigma_{\text{abs},375}$) for BC (a), primary BrC and **absorption efficiency of****
 309 **primary BrC ($\sigma_{\text{abs,pri BrC}}/\text{POA}$ is shown in shade (b), and secondary BrC, along with the $\text{C}_x\text{H}_y\text{N}_z$ and $\text{C}_x\text{H}_y\text{N}_z\text{O}_p$ fragments (c); the**
 310 **respective fraction in total for the segregated $\sigma_{\text{abs},375}$ (d-f), with direct radiation shown in shade. In each plot, the lines, dots and**
 311 **whiskers denote the median, mean and the 25th/75th percentiles at each hour respectively.**

312 4. Conclusion

313 This study apportioned the shortwave absorption of BC, primary and secondary BrC, through concurrent measurements of BC
 314 microphysical properties and OA mass spectra. The apportioned primary BrC absorption was linked with traffic and biomass
 315 burning emissions, while secondary BrC was found to be associated with an oxygenated secondary OA factor with higher
 316 nitrogen content. The enhancement of secondary BrC and decrease of primary BrC simultaneously occurred via daytime
 317 photooxidation. The results emphasize the importance of nitrogen-containing OA in contributing to BrC. These OA could
 318 primarily emit as aerosol phase, or in gas phase which requires further oxidation to be in aerosol phase to serve as BrC. The
 319 NO_x -involved chemistry is prone to add nitrogen element to the existing OA and enhance the absorptivity of chromophores.
 320 The anthropogenic NO_x emission could be therefore an important source in producing shortwave absorbing components in the
 321 atmosphere, which may offset some of the conventionally-thought photobleaching of BrC.

322 **Acknowledgments**

323 This research was supported by the National Natural Science Foundation of China (Grant No. 42175116 and 41875167),
324 National Key R&D Program of China (2019YFC0214703).

325 **Author contribution**

326 D.L., X.J. and Qian L. prepared and designed the observation. D.L., Qian L., X.J and P.T. initiated the field campaign and
327 conducted the measurements. Qian L., D.L. P.T., Y.W., S.L. and K.H. contributed to the data analysis. Qian L., H.M., L.R.,
328 B.K., D.D. and S.K. provided technical support and assistance. Qian L. and D.L. wrote the manuscript. All authors read and
329 approved the final manuscript.

330

331 **References**

- 332 Aiken, A. C., Salcedo, D., Cubison, M. J., Huffman, J. A., DeCarlo, P. F., Ulbrich, I. M., Docherty, K. S., Sueper, D., Kimmel,
333 J. R., Worsnop, D. R., Trimborn, A., Northway, M., Stone, E. A., Schauer, J. J., Volkamer, R. M., Fortner, E., de Foy, B., Wang,
334 J., Laskin, A., Shutthanandan, V., Zheng, J., Zhang, R., Gaffney, J., Marley, N. A., Paredes-Miranda, G., Arnott, W. P., Molina,
335 L. T., Sosa, G., and Jimenez, J. L.: Mexico City aerosol analysis during MILAGRO using high resolution aerosol mass
336 spectrometry at the urban supersite (T0) - Part 1: Fine particle composition and organic source apportionment, *Atmos Chem*
337 *Phys*, 9, 6633-6653, 10.5194/acp-9-6633-2009, 2009.
- 338 Andreae, M. O. and Crutzen, P. J.: Atmospheric aerosols: Biogeochemical sources and role in atmospheric chemistry, *Science*,
339 276, 1052-1058, doi:10.1126/science.276.5315.1052, 1997.
- 340 Bahadur, R., Praveen, P. S., Xu, Y., and Ramanathan, V.: Solar absorption by elemental and brown carbon determined from
341 spectral observations, *Proceedings of the National Academy of Sciences of the United States of America*, 109, 17366-17371,
342 doi:10.1073/pnas.1205910109, 2012.
- 343 Bond, T. C.: Spectral dependence of visible light absorption by carbonaceous particles emitted from coal combustion,
344 *Geophysical Research Letters*, 28, 4075-4078, doi:10.1029/2001gl013652, 2001.
- 345 Bond, T. C. and Bergstrom, R. W.: Light absorption by carbonaceous particles: An investigative review, *Aerosol Science and*
346 *Technology*, 40, 27-67, doi:10.1080/02786820500421521, 2006.
- 347 Brown, S. G., Lee, T., Roberts, P. T., and Collett, J. L., Jr.: Wintertime Residential Biomass Burning in Las Vegas, Nevada;
348 Marker Components and Apportionment Methods, *Atmosphere*, 7, 10.3390/atmos7040058, 2016.
- 349 Bruns, E. A., Perraud, V., Zelenyuk, A., Ezell, M. J., Johnson, S. N., Yu, Y., Imre, D., Finlayson-Pitts, B. J., and Alexander, M.
350 L.: Comparison of FTIR and Particle Mass Spectrometry for the Measurement of Particulate Organic Nitrates, *Environmental*
351 *Science & Technology*, 44, 1056-1061, doi:10.1021/es9029864, 2010.
- 352 Canagaratna, M. R., Jimenez, J. L., Kroll, J. H., Chen, Q., Kessler, S. H., Massoli, P., Hildebrandt Ruiz, L., Fortner, E., Williams,
353 L. R., Wilson, K. R., Surratt, J. D., Donahue, N. M., Jayne, J. T., and Worsnop, D. R.: Elemental ratio measurements of organic
354 compounds using aerosol mass spectrometry: characterization, improved calibration, and implications, *Atmospheric Chemistry*
355 *and Physics*, 15, 253-272, doi:10.5194/acp-15-253-2015, 2015.
- 356 Canagaratna, M. R., Jayne, J. T., Jimenez, J. L., Allan, J. D., Alfarra, M. R., Zhang, Q., Onasch, T. B., Drewnick, F., Coe, H.,
357 Middlebrook, A., Delia, A., Williams, L. R., Trimborn, A. M., Northway, M. J., DeCarlo, P. F., Kolb, C. E., Davidovits, P., and
358 Worsnop, D. R.: Chemical and microphysical characterization of ambient aerosols with the aerodyne aerosol mass spectrometer,
359 *Mass Spectrometry Reviews*, 26, 185-222, doi:10.1002/mas.20115, 2007.
- 360 Cheng, Y., Engling, G., He, K. B., Duan, F. K., Ma, Y. L., Du, Z. Y., Liu, J. M., Zheng, M., and Weber, R. J.: Biomass burning
361 contribution to Beijing aerosol, *Atmospheric Chemistry and Physics*, 13, 7765-7781, doi:10.5194/acp-13-7765-2013, 2013.
- 362 Coury, C. and Dillner, A. M.: A method to quantify organic functional groups and inorganic compounds in ambient aerosols
363 using attenuated total reflectance FTIR spectroscopy and multivariate chemometric techniques, *Atmospheric Environment*, 42,

364 5923-5932, doi:10.1016/j.atmosenv.2008.03.026, 2008.

365 Crilley, L. R., Bloss, W. J., Yin, J., Beddows, D. C. S., Harrison, R. M., Allan, J. D., Young, D. E., Flynn, M., Williams, P.,
366 Zotter, P., Prevot, A. S. H., Heal, M. R., Barlow, J. F., Halios, C. H., Lee, J. D., Szidat, S., and Mohr, C.: Sources and
367 contributions of wood smoke during winter in London: assessing local and regional influences, *Atmos Chem Phys*, 15, 3149-
368 3171, 10.5194/acp-15-3149-2015, 2015.

369 Cubison, M. J., Ortega, A. M., Hayes, P. L., Farmer, D. K., Day, D., Lechner, M. J., Brune, W. H., Apel, E., Diskin, G. S.,
370 Fisher, J. A., Fuelberg, H. E., Hecobian, A., Knapp, D. J., Mikoviny, T., Riemer, D., Sachse, G. W., Sessions, W., Weber, R. J.,
371 Weinheimer, A. J., Wisthaler, A., and Jimenez, J. L.: Effects of aging on organic aerosol from open biomass burning smoke in
372 aircraft and laboratory studies, *Atmos Chem Phys*, 11, 12049-12064, 10.5194/acp-11-12049-2011, 2011.

373 DeCarlo, P. F., Ulbrich, I. M., Crounse, J., de Foy, B., Dunlea, E. J., Aiken, A. C., Knapp, D., Weinheimer, A. J., Campos, T.,
374 Wennberg, P. O., and Jimenez, J. L.: Investigation of the sources and processing of organic aerosol over the Central Mexican
375 Plateau from aircraft measurements during MILAGRO, *Atmospheric Chemistry and Physics*, 10, 5257-5280, doi:10.5194/acp-
376 10-5257-2010, 2010.

377 DeWitt, H. L., Hellebust, S., Temime-Roussel, B., Ravier, S., Polo, L., Jacob, V., Buisson, C., Charron, A., Andre, M., Pasquier,
378 A., Besombes, J. L., Jaffrezo, J. L., Wortham, H., and Marchand, N.: Near-highway aerosol and gas-phase measurements in a
379 high-diesel environment, *Atmospheric Chemistry and Physics*, 15, 4373-4387, doi:10.5194/acp-15-4373-2015, 2015.

380 Ding, S., Liu, D., Zhao, D., Hu, K., Tian, P., Zhou, W., Huang, M., Yang, Y., Wang, F., Sheng, J., Liu, Q., Kong, S., Cui, P.,
381 Huang, Y., He, H., Coe, H., and Ding, D.: Size-Related Physical Properties of Black Carbon in the Lower Atmosphere over
382 Beijing and Europe, *Environmental Science & Technology*, 53, 11112-11121, doi:10.1021/acs.est.9b03722, 2019.

383 Draxier, R. R. and Hess, G. D.: An overview of the HYSPLIT_4 modelling system for trajectories, dispersion and deposition,
384 *Australian Meteorological Magazine*, 47, 295-308, 1998.

385 Drinovec, L., Mo?nik, G., Zotter, P., Prév?t, A. S. H., Ruckstuhl, C., Coz, E., Rupakheti, M., Sciare, J., Müller, T., and
386 Wiedensohler, A.: The "dual-spot" Aethalometer: an improved measurement of aerosol black carbon with real-time loading
387 compensation, *Atmospheric Measurement Techniques*, 8, 1965-1979, 2015.

388 Ehn, M., Thornton, J. A., Kleist, E., Sipila, M., Junninen, H., Pullinen, I., Springer, M., Rubach, F., Tillmann, R., Lee, B.,
389 Lopez-Hilfiker, F., Andres, S., Acir, I.-H., Rissanen, M., Jokinen, T., Schobesberger, S., Kangasluoma, J., Kontkanen, J.,
390 Nieminen, T., Kurten, T., Nielsen, L. B., Jorgensen, S., Kjaergaard, H. G., Canagaratna, M., Dal Maso, M., Berndt, T., Petaja,
391 T., Wahner, A., Kerminen, V.-M., Kulmala, M., Worsnop, D. R., Wildt, J., and Mentel, T. F.: A large source of low-volatility
392 secondary organic aerosol, *Nature*, 506, 476-+, doi:10.1038/nature13032, 2014.

393 Elser, M., Huang, R.-J., Wolf, R., Slowik, J. G., Wang, Q., Canonaco, F., Li, G., Bozzetti, C., Daellenbach, K. R., Huang, Y.,
394 Zhang, R., Li, Z., Cao, J., Baltensperger, U., El-Haddad, I., and Prevot, A. S. H.: New insights into PM_{2.5} chemical
395 composition and sources in two major cities in China during extreme haze events using aerosol mass spectrometry, *Atmos
396 Chem Phys*, 16, 3207-3225, 10.5194/acp-16-3207-2016, 2016.

397 Finewax, Z., de Gouw, J. A., and Ziemann, P. J.: Identification and Quantification of 4-Nitrocatechol Formed from OH and

398 NO₃ Radical-Initiated Reactions of Catechol in Air in the Presence of NO_x: Implications for Secondary Organic Aerosol
399 Formation from Biomass Burning, *Environmental Science & Technology*, 52, 1981-1989, doi:10.1021/acs.est.7b05864, 2018.

400 Forrister, H., Liu, J., Scheuer, E., Dibb, J., Ziemba, L., Thornhill, K. L., Anderson, B., Diskin, G., Perring, A. E., Schwarz, J.
401 P., Campuzano-Jost, P., Day, D. A., Palm, B. B., Jimenez, J. L., Nenes, A., and Weber, R. J.: Evolution of brown carbon in
402 wildfire plumes, *Geophysical Research Letters*, 42, 4623-4630, doi:10.1002/2015gl063897, 2015.

403 Gentner, D. R., Isaacman, G., Worton, D. R., Chan, A. W. H., Dallmann, T. R., Davis, L., Liu, S., Day, D. A., Russell, L. M.,
404 Wilson, K. R., Weber, R., Guha, A., Harley, R. A., and Goldstein, A. H.: Elucidating secondary organic aerosol from diesel and
405 gasoline vehicles through detailed characterization of organic carbon emissions, *Proceedings of the National Academy of
406 Sciences of the United States of America*, 109, 18318-18323, doi:10.1073/pnas.1212272109, 2012.

407 Gentner, D. R., Jathar, S. H., Gordon, T. D., Bahreini, R., Day, D. A., El Haddad, I., Hayes, P. L., Pieber, S. M., Platt, S. M.,
408 de Gouw, J., Goldstein, A. H., Harley, R. A., Jimenez, J. L., Prevot, A. S. H., and Robinson, A. L.: Review of Urban Secondary
409 Organic Aerosol Formation from Gasoline and Diesel Motor Vehicle Emissions, *Environmental Science & Technology*, 51,
410 1074-1093, doi:10.1021/acs.est.6b04509, 2017.

411 Hayes, P. L., Ortega, A. M., Cubison, M. J., Froyd, K. D., Zhao, Y., Cliff, S. S., Hu, W. W., Toohey, D. W., Flynn, J. H., Lefer,
412 B. L., Grossberg, N., Alvarez, S., Rappenglueck, B., Taylor, J. W., Allan, J. D., Holloway, J. S., Gilman, J. B., Kuster, W. C.,
413 De Gouw, J. A., Massoli, P., Zhang, X., Liu, J., Weber, R. J., Corrigan, A. L., Russell, L. M., Isaacman, G., Worton, D. R.,
414 Kreisberg, N. M., Goldstein, A. H., Thalman, R., Waxman, E. M., Volkamer, R., Lin, Y. H., Surratt, J. D., Kleindienst, T. E.,
415 Offenberg, J. H., Dusanter, S., Griffith, S., Stevens, P. S., Brioude, J., Angevine, W. M., and Jimenez, J. L.: Organic aerosol
416 composition and sources in Pasadena, California, during the 2010 CalNex campaign, *Journal of Geophysical Research-
417 Atmospheres*, 118, 9233-9257, 10.1002/jgrd.50530, 2013.

418 Hu, K., Liu, D., Tian, P., Wu, Y., Deng, Z., Wu, Y., Zhao, D., Li, R., Sheng, J., Huang, M., Ding, D., Li, W., Wang, Y., and Wu,
419 Y.: Measurements of the Diversity of Shape and Mixing State for Ambient Black Carbon Particles, *Geophysical Research
420 Letters*, 48, 10.1029/2021gl094522, 2021.

421 Hu, W., Hu, M., Hu, W.-W., Zheng, J., Chen, C., Wu, Y., and Guo, S.: Seasonal variations in high time-resolved chemical
422 compositions, sources, and evolution of atmospheric submicron aerosols in the megacity Beijing, *Atmos Chem Phys*, 17, 9979-
423 10000, 10.5194/acp-17-9979-2017, 2017.

424 Huang, D. D., Zhu, S., An, J., Wang, Q., Qiao, L., Zhou, M., He, X., Ma, Y., Sun, Y., Huang, C., Yu, J. Z., and Zhang, Q.:
425 Comparative Assessment of Cooking Emission Contributions to Urban Organic Aerosol Using Online Molecular Tracers and
426 Aerosol Mass Spectrometry Measurements, *Environmental Science & Technology*, 55, 14526-14535, 10.1021/acs.est.1c03280,
427 2021.

428 Huffman, J. A., Docherty, K. S., Aiken, A. C., Cubison, M. J., Ulbrich, I. M., DeCarlo, P. F., Sueper, D., Jayne, J. T., Worsnop,
429 D. R., Ziemann, P. J., and Jimenez, J. L.: Chemically-resolved aerosol volatility measurements from two megacity field studies,
430 *Atmospheric Chemistry and Physics*, 9, 7161-7182, doi:10.5194/acp-9-7161-2009, 2009.

431 Jacobson, M. Z.: Isolating nitrated and aromatic aerosols and nitrated aromatic gases as sources of ultraviolet light absorption,

432 Journal of Geophysical Research-Atmospheres, 104, 3527-3542, doi:10.1029/1998jd100054, 1999.

433 Jimenez, J. L., Canagaratna, M. R., Donahue, N. M., Prevot, A. S. H., Zhang, Q., Kroll, J. H., DeCarlo, P. F., Allan, J. D., Coe,
434 H., Ng, N. L., Aiken, A. C., Docherty, K. S., Ulbrich, I. M., Grieshop, A. P., Robinson, A. L., Duplissy, J., Smith, J. D., Wilson,
435 K. R., Lanz, V. A., Hueglin, C., Sun, Y. L., Tian, J., Laaksonen, A., Raatikainen, T., Rautiainen, J., Vaattovaara, P., Ehn, M.,
436 Kulmala, M., Tomlinson, J. M., Collins, D. R., Cubison, M. J., Dunlea, E. J., Huffman, J. A., Onasch, T. B., Alfarra, M. R.,
437 Williams, P. I., Bower, K., Kondo, Y., Schneider, J., Drewnick, F., Borrmann, S., Weimer, S., Demerjian, K., Salcedo, D.,
438 Cottrell, L., Griffin, R., Takami, A., Miyoshi, T., Hatakeyama, S., Shimono, A., Sun, J. Y., Zhang, Y. M., Dzepina, K., Kimmel,
439 J. R., Sueper, D., Jayne, J. T., Herndon, S. C., Trimborn, A. M., Williams, L. R., Wood, E. C., Middlebrook, A. M., Kolb, C.
440 E., Baltensperger, U., and Worsnop, D. R.: Evolution of Organic Aerosols in the Atmosphere, *Science*, 326, 1525-1529,
441 doi:10.1126/science.1180353, 2009.

442 Keyte, I. J., Albinet, A., and Harrison, R. M.: On-road traffic emissions of polycyclic aromatic hydrocarbons and their oxy-
443 and nitro-derivative compounds measured in road tunnel environments, *Science of the Total Environment*, 566, 1131-1142,
444 doi:10.1016/j.scitotenv.2016.05.152, 2016.

445 Laborde, M., Schnaiter, M., Linke, C., Saathoff, H., Naumann, K. H., Moehler, O., Berlenz, S., Wagner, U., Taylor, J. W., Liu,
446 D., Flynn, M., Allan, J. D., Coe, H., Heimerl, K., Dahlkoetter, F., Weinzierl, B., Wollny, A. G., Zannata, M., Cozic, J., Laj, P.,
447 Hitzenberger, R., Schwarz, J. P., and Gysel, M.: Single Particle Soot Photometer intercomparison at the AIDA chamber,
448 *Atmospheric Measurement Techniques*, 5, 3077-3097, doi:10.5194/amt-5-3077-2012, 2012.

449 Laskin, A., Laskin, J., and Nizkorodov, S. A.: Chemistry of Atmospheric Brown Carbon, *Chemical Reviews*, 115, 4335-4382,
450 doi:10.1021/cr5006167, 2015.

451 Liebmann, J., Sobanski, N., Schuladen, J., Karu, E., Hellen, H., Hakola, H., Zha, Q., Ehn, M., Riva, M., Heikkinen, L.,
452 Williams, J., Fischer, H., Lelieveld, J., and Crowley, J. N.: Alkyl nitrates in the boreal forest: formation via the NO₃-, OH- and
453 O₃-induced oxidation of biogenic volatile organic compounds and ambient lifetimes, *Atmospheric Chemistry and Physics*,
454 19, 10391-10403, doi:10.5194/acp-19-10391-2019, 2019.

455 Lin, P., Liu, J., Shilling, J. E., Kathmann, S. M., Laskin, J., and Laskin, A.: Molecular characterization of brown carbon (BrC)
456 chromophores in secondary organic aerosol generated from photo-oxidation of toluene, *Physical Chemistry Chemical Physics*,
457 17, 23312-23325, doi:10.1039/c5cp02563j, 2015.

458 Liu, D., He, C., Schwarz, J. P., and Wang, X.: Lifecycle of light-absorbing carbonaceous aerosols in the atmosphere, *npj*
459 *Climate and Atmospheric Science*, 3, 40, doi:10.1038/s41612-020-00145-8, 2020.

460 Liu, D., Taylor, J. W., Young, D. E., Flynn, M. J., Coe, H., and Allan, J. D.: The effect of complex black carbon microphysics
461 on the determination of the optical properties of brown carbon, *Geophysical Research Letters*, 42, 613-619,
462 doi:10.1002/2014gl062443, 2015a.

463 Liu, D., Allan, J. D., Young, D. E., Coe, H., Beddows, D., Fleming, Z. L., Flynn, M. J., Gallagher, M. W., Harrison, R. M., Lee,
464 J., Prevot, A. S. H., Taylor, J. W., Yin, J., Williams, P. I., and Zotter, P.: Size distribution, mixing state and source apportionment
465 of black carbon aerosol in London during wintertime, *Atmospheric Chemistry and Physics*, 14, 10061-10084, doi:10.5194/acp-

466 14-10061-2014, 2014.

467 Liu, D., Joshi, R., Wang, J., Yu, C., Allan, J. D., Coe, H., Flynn, M. J., Xie, C., Lee, J., Squires, F., Kotthaus, S., Grimmond,
468 S., Ge, X., Sun, Y., and Fu, P.: Contrasting physical properties of black carbon in urban Beijing between winter and summer,
469 Atmospheric Chemistry and Physics, 19, 6749-6769, doi:10.5194/acp-19-6749-2019, 2019a.

470 Liu, D., Joshi, R., Wang, J., Yu, C., Allan, J. D., Coe, H., Flynn, M. J., Xie, C., Lee, J., Squires, F., Kotthaus, S., Grimmond,
471 S., Ge, X., Sun, Y., and Fu, P.: Contrasting physical properties of black carbon in urban Beijing between winter and summer,
472 Atmos. Chem. Phys., 19, 6749-6769, doi:10.5194/acp-19-6749-2019, 2019b.

473 Liu, D., Li, S., Hu, D., Kong, S., Cheng, Y., Wu, Y., Ding, S., Hu, K., Zheng, S., Yan, Q., Zheng, H., Zhao, D., Tian, P., Ye, J.,
474 Huang, M., and Ding, D.: Evolution of Aerosol Optical Properties from Wood Smoke in Real Atmosphere Influenced by
475 Burning Phase and Solar Radiation, Environmental Science & Technology, 55, 5677-5688, doi:10.1021/acs.est.0c07569, 2021.

476 Liu, F., Zhang, Q., Tong, D., Zheng, B., Li, M., Huo, H., and He, K. B.: High-resolution inventory of technologies, activities,
477 and emissions of coal-fired power plants in China from 1990 to 2010, Atmospheric Chemistry and Physics, 15, 13299-13317,
478 doi:10.5194/acp-15-13299-2015, 2015b.

479 Liu, J., Mauzerall, D. L., Chen, Q., Zhang, Q., Song, Y., Peng, W., Klimont, Z., Qiu, X., Zhang, S., Hu, M., Lin, W., Smith, K.
480 R., and Zhu, T.: Air pollutant emissions from Chinese households: A major and underappreciated ambient pollution source,
481 Proceedings of the National Academy of Sciences of the United States of America, 113, 7756-7761,
482 doi:10.1073/pnas.1604537113, 2016.

483 Liu, P. F., Abdelmalki, N., Hung, H. M., Wang, Y., Brune, W. H., and Martin, S. T.: Ultraviolet and visible complex refractive
484 indices of secondary organic material produced by photooxidation of the aromatic compounds toluene and m-xylene,
485 Atmospheric Chemistry and Physics, 15, 1435-1446, doi:10.5194/acp-15-1435-2015, 2015c.

486 Makra, L., Matyasovszky, I., Guba, Z., Karatzas, K., and Anttila, P.: Monitoring the long-range transport effects on urban
487 PM10 levels using 3D clusters of backward trajectories, Atmospheric Environment, 45, 2630-2641,
488 doi:10.1016/j.atmosenv.2011.02.068, 2011.

489 Mohr, C., DeCarlo, P. F., Heringa, M. F., Chirico, R., Slowik, J. G., Richter, R., Reche, C., Alastuey, A., Querol, X., Seco, R.,
490 Penuelas, J., Jimenez, J. L., Crippa, M., Zimmermann, R., Baltensperger, U., and Prevot, A. S. H.: Identification and
491 quantification of organic aerosol from cooking and other sources in Barcelona using aerosol mass spectrometer data,
492 Atmospheric Chemistry and Physics, 12, 1649-1665, doi:10.5194/acp-12-1649-2012, 2012.

493 Nakayama, T., Sato, K., Matsumi, Y., Imamura, T., Yamazaki, A., and Uchiyama, A.: Wavelength and NO_x dependent complex
494 refractive index of SOAs generated from the photooxidation of toluene, Atmospheric Chemistry and Physics, 13, 531-545,
495 doi:10.5194/acp-13-531-2013, 2013.

496 Ng, N. L., Kwan, A. J., Surratt, J. D., Chan, A. W. H., Chhabra, P. S., Sorooshian, A., Pye, H. O. T., Crounse, J. D., Wennberg,
497 P. O., Flagan, R. C., and Seinfeld, J. H.: Secondary organic aerosol (SOA) formation from reaction of isoprene with nitrate
498 radicals (NO₃), Atmospheric Chemistry and Physics, 8, 4117-4140, doi:10.5194/acp-8-4117-2008, 2008.

499 Paatero, P. and Tapper, U.: POSITIVE MATRIX FACTORIZATION - A NONNEGATIVE FACTOR MODEL WITH

500 OPTIMAL UTILIZATION OF ERROR-ESTIMATES OF DATA VALUES, *Environmetrics*, 5, 111-126,
501 doi:10.1002/env.3170050203, 1994.

502 Pachon, J. E., Weber, R. J., Zhang, X., Mulholland, J. A., and Russell, A. G.: Revising the use of potassium (K) in the source
503 apportionment of PM_{2.5}, *Atmospheric Pollution Research*, 4, 14-21, 10.5094/apr.2013.002, 2013.

504 Rizzo, L. V., Artaxo, P., Mueller, T., Wiedensohler, A., Paixao, M., Cirino, G. G., Arana, A., Swietlicki, E., Roldin, P., Fors, E.
505 O., Wiedemann, K. T., Leal, L. S. M., and Kulmala, M.: Long term measurements of aerosol optical properties at a primary
506 forest site in Amazonia, *Atmospheric Chemistry and Physics*, 13, 2391-2413, doi:10.5194/acp-13-2391-2013, 2013.

507 Rollins, A. W., Browne, E. C., Min, K. E., Pusede, S. E., Wooldridge, P. J., Gentner, D. R., Goldstein, A. H., Liu, S., Day, D.
508 A., Russell, L. M., and Cohen, R. C.: Evidence for NO_x Control over Nighttime SOA Formation, *Science*, 337, 1210-1212,
509 doi:10.1126/science.1221520, 2012.

510 Satish, R. and Rastogi, N.: On the Use of Brown Carbon Spectra as a Tool to Understand Their Broader Composition and
511 Characteristics: A Case Study from Crop-residue Burning Samples, *Acs Omega*, 4, 1847-1853, 10.1021/acsomega.8b02637,
512 2019.

513 Satish, R., Shamjad, P., Thamban, N., Tripathi, S., and Rastogi, N.: Temporal Characteristics of Brown Carbon over the Central
514 Indo-Gangetic Plain, *Environmental Science & Technology*, 51, 6765-6772, 10.1021/acs.est.7b00734, 2017.

515 Schnitzler, E. G., Liu, T., Hems, R. F., and Abbatt, J. P. D.: Emerging investigator series: heterogeneous OH oxidation of
516 primary brown carbon aerosol: effects of relative humidity and volatility, *Environmental Science-Processes & Impacts*, 22,
517 2162-2171, 10.1039/d0em00311e, 2020.

518 Schuetzle, D.: SAMPLING OF VEHICLE EMISSIONS FOR CHEMICAL-ANALYSIS AND BIOLOGICAL TESTING,
519 *Environmental Health Perspectives*, 47, 65-80, doi:10.2307/3429500, 1983.

520 Shen, G., Ru, M., Du, W., Zhu, X., Zhong, Q., Chen, Y., Shen, H., Yun, X., Meng, W., Liu, J., Cheng, H., Hu, J., Guan, D., and
521 Tao, S.: Impacts of air pollutants from rural Chinese households under the rapid residential energy transition, *Nature*
522 *Communications*, 10, doi:10.1038/s41467-019-11453-w, 2019.

523 Siemens, K., Morales, A., He, Q., Li, C., Hettiyadura, A. P. S., Rudich, Y., and Laskin, A.: Molecular Analysis of Secondary
524 Brown Carbon Produced from the Photooxidation of Naphthalene, *Environmental science & technology*, 56, 3340-3353,
525 doi:10.1021/acs.est.1c03135, 2022.

526 Sun, Y., Jiang, Q., Wang, Z., Fu, P., Li, J., Yang, T., and Yin, Y.: Investigation of the sources and evolution processes of severe
527 haze pollution in Beijing in January 2013, *Journal of Geophysical Research-Atmospheres*, 119, 4380-4398,
528 doi:10.1002/2014jd021641, 2014.

529 Sun, Y., Du, W., Fu, P., Wang, Q., Li, J., Ge, X., Zhang, Q., Zhu, C., Ren, L., Xu, W., Zhao, J., Han, T., Worsnop, D. R., and
530 Wang, Z.: Primary and secondary aerosols in Beijing in winter: sources, variations and processes, *Atmos Chem Phys*, 16, 8309-
531 8329, 10.5194/acp-16-8309-2016, 2016.

532 Sun, Y. L., Zhang, Q., Schwab, J. J., Chen, W. N., Bae, M. S., Lin, Y. C., Hung, H. M., and Demerjian, K. L.: A case study of
533 aerosol processing and evolution in summer in New York City, *Atmos Chem Phys*, 11, 12737-12750, 10.5194/acp-11-12737-

534 2011, 2011a.

535 Sun, Y. L., Zhang, Q., Schwab, J. J., Demerjian, K. L., Chen, W. N., Bae, M. S., Hung, H. M., Hogrefe, O., Frank, B., Rattigan,
536 O. V., and Lin, Y. C.: Characterization of the sources and processes of organic and inorganic aerosols in New York city with a
537 high-resolution time-of-flight aerosol mass spectrometer, *Atmospheric Chemistry and Physics*, 11, 1581-1602,
538 doi:10.5194/acp-11-1581-2011, 2011b.

539 Taylor, J. W., Allan, J. D., Liu, D., Flynn, M., Weber, R., Zhang, X., Lefer, B. L., Grossberg, N., Flynn, J., and Coe, H.:
540 Assessment of the sensitivity of core/shell parameters derived using the single-particle soot photometer to density and
541 refractive index, *Atmospheric Measurement Techniques*, 8, 1701-1718, doi:10.5194/amt-8-1701-2015, 2015.

542 Tian, P., Liu, D., Zhao, D., Yu, C., Liu, Q., Huang, M., Deng, Z., Ran, L., Wu, Y., Ding, S., Hu, K., Zhao, G., Zhao, C., and
543 Ding, D.: In situ vertical characteristics of optical properties and heating rates of aerosol over Beijing, *Atmospheric Chemistry
544 and Physics*, 20, 2603-2622, doi:10.5194/acp-20-2603-2020, 2020.

545 Ulbrich, I. M., Canagaratna, M. R., Zhang, Q., Worsnop, D. R., and Jimenez, J. L.: Interpretation of organic components from
546 Positive Matrix Factorization of aerosol mass spectrometric data, *Atmospheric Chemistry and Physics*, 9, 2891-2918,
547 doi:10.5194/acp-9-2891-2009, 2009.

548 Updyke, K. M., Nguyen, T. B., and Nizkorodov, S. A.: Formation of brown carbon via reactions of ammonia with secondary
549 organic aerosols from biogenic and anthropogenic precursors, *Atmospheric Environment*, 63, 22-31,
550 doi:10.1016/j.atmosenv.2012.09.012, 2012.

551 Wang, Q., Han, Y., Ye, J., Liu, S., Pongpiachan, S., Zhang, N., Han, Y., Tian, J., Wu, C., Long, X., Zhang, Q., Zhang, W., Zhao,
552 Z., and Cao, J.: High Contribution of Secondary Brown Carbon to Aerosol Light Absorption in the Southeastern Margin of
553 Tibetan Plateau, *Geophysical Research Letters*, 46, 4962-4970, 10.1029/2019gl082731, 2019a.

554 Wang, Q., Cao, J., Han, Y., Tian, J., Zhang, Y., Pongpiachan, S., Zhang, Y., Li, L., Niu, X., Shen, Z., Zhao, Z., Tipmanee, D.,
555 Bunsomboonsakul, S., Chen, Y., and Sun, J.: Enhanced light absorption due to the mixing state of black carbon in fresh biomass
556 burning emissions, *Atmospheric Environment*, 180, 184-191, doi:10.1016/j.atmosenv.2018.02.049, 2018.

557 Wang, X., Heald, C. L., Ridley, D. A., Schwarz, J. P., Spackman, J. R., Perring, A. E., Coe, H., Liu, D., and Clarke, A. D.:
558 Exploiting simultaneous observational constraints on mass and absorption to estimate the global direct radiative forcing of
559 black carbon and brown carbon, *Atmospheric Chemistry and Physics*, 14, 10989-11010, doi:10.5194/acp-14-10989-2014, 2014.

560 Wang, Y., Hu, M., Wang, Y., Zheng, J., Shang, D., Yang, Y., Liu, Y., Li, X., Tang, R., Zhu, W., Du, Z., Wu, Y., Guo, S., Wu, Z.,
561 Lou, S., Hallquist, M., and Yu, J. Z.: The formation of nitro-aromatic compounds under high NO_x and anthropogenic VOC
562 conditions in urban Beijing, China, *Atmospheric Chemistry and Physics*, 19, 7649-7665, doi:10.5194/acp-19-7649-2019,
563 2019b.

564 Wu, C. and Yu, J. Z.: Determination of primary combustion source organic carbon-to-elemental carbon (OC_{primary}/aEuro-EC)
565 ratio using ambient OC and EC measurements: secondary OC-EC correlation minimization method, *Atmos Chem Phys*, 16,
566 5453-5465, 10.5194/acp-16-5453-2016, 2016.

567 Yang, W., Zhang, Y., Wang, X., Li, S., Zhu, M., Yu, Q., Li, G., Huang, Z., Zhang, H., Wu, Z., Song, W., Tan, J., and Shao, M.:

568 Volatile organic compounds at a rural site in Beijing: influence of temporary emission control and wintertime heating,
569 Atmospheric Chemistry and Physics, 18, 12663-12682, doi:10.5194/acp-18-12663-2018, 2018.

570 Yao, Z., Shen, X., Ye, Y., Cao, X., Jiang, X., Zhang, Y., and He, K.: On-road emission characteristics of VOCs from diesel
571 trucks in Beijing, China, Atmospheric Environment, 103, 87-93, doi:10.1016/j.atmosenv.2014.12.028, 2015.

572 Zhang, Q., Worsnop, D. R., Canagaratna, M. R., and Jimenez, J. L.: Hydrocarbon-like and oxygenated organic aerosols in
573 Pittsburgh: insights into sources and processes of organic aerosols, Atmos Chem Phys, 5, 3289-3311, 10.5194/acp-5-3289-
574 2005, 2005.

575 Zhang, Q., Jimenez, J. L., Canagaratna, M. R., Ulbrich, I. M., Ng, N. L., Worsnop, D. R., and Sun, Y.: Understanding
576 atmospheric organic aerosols via factor analysis of aerosol mass spectrometry: a review, Analytical and Bioanalytical
577 Chemistry, 401, 3045-3067, doi:10.1007/s00216-011-5355-y, 2011.

578 Zhang, Q., Shen, Z., Zhang, L., Zeng, Y., Ning, Z., Zhang, T., Lei, Y., Wang, Q., Li, G., Sun, J., Westerdahl, D., Xu, H., and
579 Cao, J.: Investigation of Primary and Secondary Particulate Brown Carbon in Two Chinese Cities of Xi'an and Hong Kong in
580 Wintertime, Environmental Science & Technology, 54, 3803-3813, 10.1021/acs.est.9b05332, 2020.

581 Zhang, Y., Zhang, Q., Cheng, Y., Su, H., Li, H., Li, M., Zhang, X., Ding, A., and He, K.: Amplification of light absorption of
582 black carbon associated with air pollution, Atmospheric Chemistry and Physics, 18, 9879-9896, doi:10.5194/acp-18-9879-
583 2018, 2018.

584 Zhao, R., Lee, A. K. Y., Huang, L., Li, X., Yang, F., and Abbatt, J. P. D.: Photochemical processing of aqueous atmospheric
585 brown carbon, Atmospheric Chemistry and Physics, 15, 6087-6100, doi:10.5194/acp-15-6087-2015, 2015.

586 Zhou, S., Collier, S., Xu, J., Mei, F., Wang, J., Lee, Y.-N., Sedlacek, A. J., III, Springston, S. R., Sun, Y., and Zhang, Q.:
587 Influences of upwind emission sources and atmospheric processing on aerosol chemistry and properties at a rural location in
588 the Northeastern US, Journal of Geophysical Research-Atmospheres, 121, 6049-6065, 10.1002/2015jd024568, 2016.

589
590